ELSEVIER

Advances in Water Resources 23 (2000) 427–439

Advances in Water Resources

The dynamic role of root-water uptake in coupling potential to actual transpiration

Chun-Ta Lai [a,b,*], Gabriel Katul [a,b]

[a] School of the Environment, Duke University, Box 90328, Durham, NC 27708-0328, USA
[b] Center for Hydrologic Science, Duke University, Durham, NC 27707, USA

Received 7 May 1998; received in revised form 12 January 1999; accepted 10 April 1999

Abstract

The relationship between actual (E_{act}) and potential (E_p) transpiration above a grass-covered forest clearing was investigated numerically and experimentally from simultaneous measurements of soil moisture content profiles, mean meteorological conditions, turbulent heat and water vapor fluxes in the atmospheric surface layer, and soil hydraulic properties for two drying periods. The relationship between E_{act}/E_p was found to be approximately constant and insensitive to variability in near-surface soil moisture content. To explore this near-constant E_{act}/E_p, a model that relates potential and actual transpiration and accounts for root-uptake efficiency, potential transpiration rate, and root-density distribution was proposed and field-tested. The total amount of water consumed by the root system was integrated and compared with eddy-correlation latent heat flux measurements (field scale) and total water storage changes (local scale). Model calculations suggested that the deeper and more efficient roots are primarily responsible for the total water loss within the root zone when the near-surface soil layer approaches their wilting point.

Keywords: Root water uptake; Root density; Root efficiency; Transpiration; Potential evaporation; Infiltration

1. Introduction

Quantifying soil moisture content redistribution within a stratified soil in the presence of a rooting system continues to be a practical problem in surface hydrology and climate research [14,30,34,46,58]. The basic approach to describe soil moisture content dynamics in the root-zone follows a modified one-dimensional continuity equation [18,36], given by

$$\frac{\partial\theta(z,t)}{\partial t} = -\frac{\partial q(z,t)}{\partial z} - S(z,t), \tag{1}$$

where θ is the soil moisture content at depth z (positive downward) and time t, q is the Darcian water flux, and S is the water sink by the plant-root system in a soil layer of thickness dz, and is related to the actual transpiration (E_{act}) via

$$E_{act}(t) = \int_0^L S(z,t)\,\mathrm{d}z, \tag{2}$$

where L is the root-zone depth. In order to model $\theta(z,t)$ within the root-zone, a complete description of $S(z,t)$ is necessary. Typically, $S(z,t)$ depends on root-density distribution [19,24,31,43,45,55], relative proportion of active roots responsible for water uptake [50], soil moisture content [18,57], and atmospheric demand [43], among other things [20,51,52], and is difficult to implement in practical soil-plant-atmosphere models. In addition, much of the root properties (e.g. root-density, proportion of active roots, etc.) are not stationary [3,4,16,21,33]. In climate and hydrologic models, it is difficult to explicitly describe (or resolve) all the complex processes influencing $S(z,t)$. Hence, in such models, E_{act} is typically modeled or estimated using

$$E_{act} = \beta(\theta)E_p, \tag{3}$$

where β is an empirical reduction function $\beta(\theta) \in [0,1]$ [2]. More elaborate resistance formulations such as the Penman–Monteith (see [5,32] for reviews) are widely used to estimate E_{act}; however, estimating E_{act} alone only permits computing depth-averaged $S(z,t)$ over the

* Corresponding author. School of the Environment, Duke University, Box 90328, Durham, NC 27708-0328, USA. Tel.: +1-919-613-8068; fax: +1-919-684-8741.
E-mail address: cl9@duke.edu (C.-T. Lai)

0309-1708/00/$ - see front matter
PII: S0309-1708(99)00023-8

entire L. That is, with such E_{act} model estimates, only depth-averaged soil moisture content over the entire L can be calculated using

$$\frac{\partial}{\partial t}\int_0^L \theta(z,t)\,dz = -(q(L,t) - q(0,t)) - E_{act}(t). \quad (4)$$

Such an approach cannot permit any detailed accounting for the large vertical variability in observed θ within the root-zone. To permit elementary accounting of such large vertical gradients in soil moisture in climate models, Dickinson et al. [14] proposed that relative rates of water extraction from different soil layers be strictly represented in terms of root-density distribution. Whether such a representation is realistic remains to be investigated given the strong experimental evidence against the Dickinson et al. [14] proposition [22,26,37,52]. On the other extreme, Clausnitzer and Hopmans [12] and Somma et al. [53] proposed a transient model for root growth as a function of mechanical soil strength, soil temperature, solute concentration, and a branching pattern described by root age and empirically specified impedance factors. Such an approach can reproduce observed patterns in root-growth and changes in root-density; however, the model parameters of such an approach are not known a priori and cannot be determined from quantities resolved by hydrologic and climate models. Hence, there is a clear need for an intermediate class of models that combine many observed features about root-water uptake yet are sufficiently simple to incorporate in practical hydrologic and climate models.

In this study, a model for $S(z,t)$ that accounts for vertical variability in root-density distribution, a newly proposed root-uptake efficiency, and atmospheric demand is developed. This model is then combined with measured soil moisture content time series at multiple depths to investigate mechanisms responsible for root activity at different soil layers in relation to soil moisture. The outcome of this study will help guide future multi-level soil-vegetation-atmosphere models in which vertical variability of root-zone soil moisture content is an intrinsic component.

2. Theory

2.1. Water movement in soil

In order to describe $\theta(z,t)$ within the root-zone, the two terms on the right-hand side of Eq. (1) require parameterizations. The first term can be quantified using

$$q = -k(\theta)\left(1 + \frac{\partial \Psi(\theta)}{\partial z}\right), \quad (5)$$

where $k(\theta)$ is the hydraulic conductivity function, and $\Psi(\theta)$ is the soil matric potential.

The Clapp and Hornberger [11] formulation for $\Psi(\theta)$ and $k(\theta)$, given by

$$\Psi(\theta) = \Psi_s\left(\frac{\theta}{\theta_s}\right)^{-b}, \quad (6)$$

$$k(\theta) = k_s\left(\frac{\theta}{\theta_s}\right)^{2b+3} \quad (7)$$

are used, where k_s, Ψ_s are saturated hydraulic conductivity and air-entry soil tension, θ_s is the saturated moisture content, and b is an empirical parameter that varies with soil texture [10].

2.2. Root-water uptake

The sink term $S(z,t)$ in Eq. (1) varies with atmospheric demand, the "water-extracting" root-density, and root-water uptake efficiency. Many models have been proposed and tested for S (e.g. [1,19,35,36,38,47]). However, Perrochet [43] demonstrated that S can be collapsed to a canonical form given by Feddes' formulation:

$$S(\theta,z,t) = \alpha(\theta)g(z)E_p(t), \quad (8)$$

where $\alpha(\theta)$ is a root efficiency function, $g(z)$ is a root-density function, and E_p is the potential transpiration used as surrogate for atmospheric demand and is discussed in Section 2.2.3. We emphasize that (8) is still the fundamental basis for many elaborate root-zone models such as the models described in [12,53]. We have adopted the Perrochet [43] canonical form for $S(z,t)$ for two reasons:

(1) Both $g(z)$ and $\alpha(\theta)$ represent macroscopic properties of the root-soil system and, as such, inherently vary with macroscopic properties such as θ.

(2) The inherent similarity between the Perrochet and the Budyko formulation (presented in Eq. (3)) commonly used in climate and hydrologic models [7].

This similarity is best revealed upon integrating (8) and combining the integration outcome with Eq. (3) to arrive at a formulation for β given by

$$\beta = \int_0^L g(z)\,\alpha(\theta)\,dz. \quad (9)$$

2.2.1. The root-density distribution

The $g(z)$ is a rather complex function [12,13,53] and in practice, is not a priori known. The model proposed by Clausnitzer and Hopmans [12] can describe many canonical features of $g(z)$ at the expense of detailed soil and root-morphologic information. Alternatively, many field studies [19,24,27,49] found that simplified analytic expressions describe well $g(z)$ for a wide range of biomes. For illustration, the commonly used

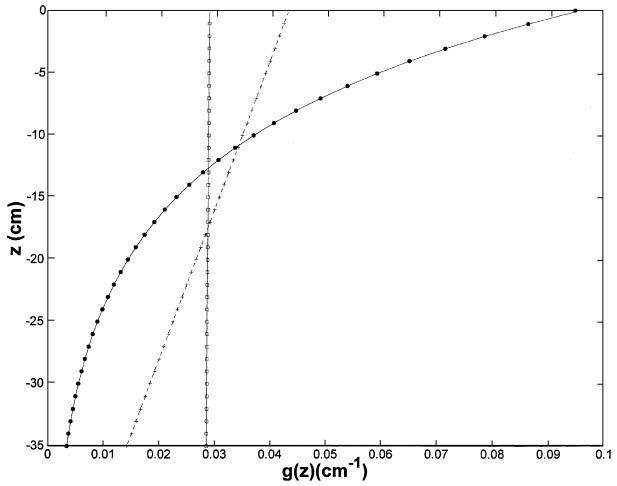

Fig. 1. Vertical variation of root density $g(z)$ with depth z as proposed by Feddes et al. [19] (square-line), Hoogland et al. [24] (plus-dashline), and Jackson et al. [27] (dot-line). The three profiles are computed for a $L = 0.35$ m rooting depth.

root-density distributions derived from such field studies are qualitatively compared in Fig. 1. In Fig. 1, the formulations of Hoogland et al. [24] and Jackson et al. [27], given by

$$g(z) = 2cz/L^2 + (1-c)/L, \tag{10a}$$

$$g(z) = -a^z \ln(a), \tag{10b}$$

respectively, are displayed for a 0.35 m rooting depth, where c is a slope parameter of the Hoogland et al. [24] model and is constrained by $-1 \leqslant c \leqslant 0$ and a (<1) is an empirical parameter of the Jackson et al. [27] model (if z is expressed in cm) and is analogous to an extinction coefficient. Notice that the equation of Hoogland et al. becomes identical to Feddes' (constant $g(z)$) model when $c = 0$. Finally, the product $g(z)$ by E_p defines the maximum root-water uptake ($= S_{max}$) at a given layer [40] if the soil moisture content is not limiting root efficiency (i.e. $\alpha = 1$). While $\theta < \theta_s$, $\alpha < 1$ and $S < S_{max}$ represent such conditions.

2.2.2. The root-efficiency function

Much of the root-efficiency models are empirical and depend on a local soil moisture or matric head formulation [36]. Here, we propose a root-efficiency function defined by

$$\alpha(\theta) = \alpha_1(\theta) \times \alpha_2(\theta), \tag{11}$$

where

$$\alpha_1(\theta) = \max\left\{ \frac{\theta}{\theta_s - \theta_w}; \frac{\int_0^z \theta(z)\,dz}{\int_0^L \theta(z)\,dz} \right\}, \tag{12}$$

$$\alpha_2(\theta) = \left(\frac{\theta - \theta_w}{\theta_s} \right)^{\gamma/(\theta-\theta_w)}, \tag{13}$$

where θ_w is the wilting point of soil moisture, and γ is an empirical constant. Unlike the Ψ-based form [12,19,36,38,39,43,53] we used a θ-based formulation [18,35] because of the large uncertainty associated with a field-measured soil water characteristic curve. We discuss our rationale for adopting the formulations in (11)–(13) next.

The proposed form in (11) decomposes the root-efficiency function into two terms: a root "shut-down" mechanism occurring around wilting point (α_2) and a maximum efficiency (α_1) when soil moisture availability is not limiting water uptake. Hence, $\alpha_2 \to 0$ when soil moisture approaches near wilting point and must gradually approach unity when $\theta \approx \theta_s$. The rate at which $\alpha_2 \to 0$ is dictated by the parameter γ of (13). In this study, we found that a $\gamma = 0.01$ ensures that $\alpha_2 \to 0$ as $\theta \approx \theta_w$ as demonstrated in Fig. 2.

In (12), α_1 is defined as the maximum of two possible uptake-efficiency limits: a local and a non-local. The non-local limit ensures that deeper roots (~0.2–0.35 m) are more efficient than top roots (~0–0.2 m) [54]. However, in the event of rapid soil wetting following a precipitation event, the top roots become more efficient ($\sim\theta/\theta_s$) if water is available and preferentially enhance their water uptake irrespective of water uptake from deeper layers. Studies [22,26] found that roots are able to preferentially uptake water from the near surface when water is freely available, but are able to adjust to near-surface drought by uptaking water from deeper layers. It is because of these previous field studies that we propose a root efficiency function to account for the switch of the root water extraction from layer to layer.

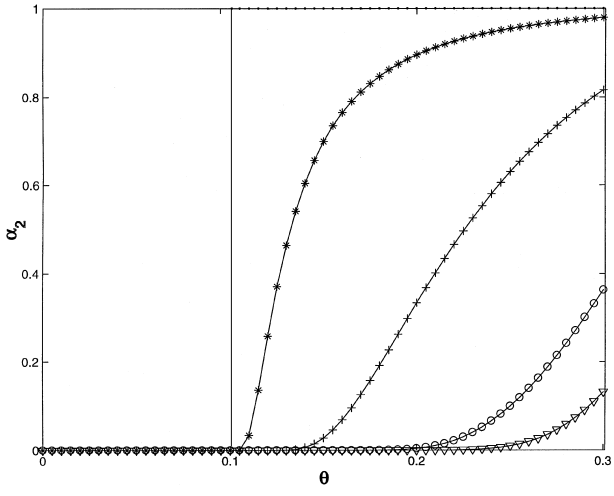

Fig. 2. Variation of root-uptake efficiency with changes in γ. Only $\alpha_2(\theta)$ (Eq. (13)) is used to illustrate root "shut-down" when $\theta \to \theta_w$ for $\gamma = 0$, 0.01, 0.1, 0.5 and 1 represented by dot, star, plus, open circle and triangle, respectively.

Finally, we note that $\alpha(\theta)$ and $g(z)$ must satisfy several constraints:

(i) The product of $\alpha(\theta)$ and $g(z)$

$$\int_0^L g(z)\alpha(\theta)\,dz \leqslant 1. \tag{14}$$

(ii) The root-density distribution

$$\int_0^L g(z)\,dz = 1. \tag{15}$$

(iii) The root-efficiency function is also bounded such that

$$\int_0^L \alpha(\theta)\,dz \leqslant 1. \tag{16}$$

2.2.3. Potential transpiration model

For potential transpiration (E_p), the Penman–Brutsaert model described in [5,28] is used. The general form of E_p is a Penman-like [42] combination equation given by

$$E_p = W(R_n - G) + (1 - W)E_A, \tag{17}$$

where E_p is the potential latent heat flux, R_n is the net radiation, G is the soil heat flux, W is a dimensionless weighing function that depends on the slope of the saturation vapor pressure–temperature curve and the psychrometric constant, and E_A is the atmospheric drying power function given by

$$E_A = \kappa u_* \rho (q^* - q_a)\left[\ln\left(\frac{z_a - d_{0v}}{z_{0v}}\right) - \psi_v\left(\frac{z_a - d_{0v}}{L_{mo}}\right)\right]^{-1}, \tag{18}$$

where $\kappa = 0.4$ is von Karman's constant, u_* is the friction velocity, ρ is the mean air density, d_{0v} is the displacement height for water vapor, z_a is the measurement height above the surface, z_{0v} is the vapor roughness height calculated using the formulation in [5] (p. 123) with a leaf area index (LAI) of 3, q_a and q^* are the actual and saturated air specific humidity, respectively. The Monin–Obukhov similarity stability correction function ψ_v depends on $(z_a - d_{0v})/L_{mo}$, where L_{mo} is the Obukhov length, defined by

$$L_{mo} = \frac{-u_*^3}{\kappa g\left[H_v/(\rho C_p T_a)\right]}, \tag{19}$$

where $H_v = \left(H + 0.61 T_a C_p E_p\right)$ is the specific flux of virtual sensible heat at the surface, C_p is the specific heat capacity at constant pressure, T_a is the mean air temperature, g is the gravitational acceleration and H is the sensible heat flux.

The friction velocity, u_*, can be determined from

$$V = \frac{u_*}{\kappa}\left[\ln\left(\frac{z_a - d_0}{z_0}\right) - \psi_m\left(\frac{z_a - d_0}{L_{mo}}\right)\right], \tag{20}$$

where V is the mean horizontal wind velocity, d_0 and z_0 are the momentum displacement height and roughness length, respectively. The functions ψ_v and ψ_m in (18) and (20) are computed by the Businger–Dyer stability correction functions with the atmospheric stability classified by L_{mo} [6,8,15]. The sensible heat flux can be computed from the surface energy budget residual using

$$H = R_n - G - E_p, \tag{21}$$

which closes the system of equations to solve for E_p.

Recently, Cahill and Parlange [9] found that the Brutsaert model [5] for *bluff-rough surfaces*, as derived from laboratory relationship between the Stanton number and the roughness Reynolds number, consistently underestimates large sensible heat flux events. It is not clear whether the Brutsaert z_{0v} formulation [5] for *permeable rough surfaces* also underestimate latent heat flux. Given the uncertainty in LAI dynamics, and the uncertainty in the parameterizations of $S(z,t)$, such a correction to E_p is minor.

2.3. Schematic integration of soil-vegetation-atmosphere system

Fig. 3 schematically shows the dynamic linkage between atmospheric demand and the soil-vegetation-system. Input parameters for potential transpiration are measured mean meteorological variables (mean air temperature, mean relative humidity, mean wind velocity, net radiation, and soil heat flux). The computed E_p is then combined with soil properties (hydraulic conductivity, saturated soil moisture, air-entry soil tension and the empirical soil parameter b) and serves as an input for the root-water uptake $S(z,t)$ model and subsequent soil water redistribution via the modified Richards' equation. During precipitation events

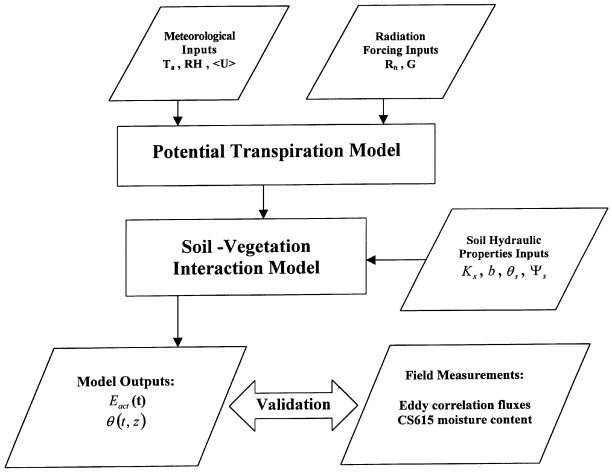

Fig. 3. Schematic linkage between micrometeorological inputs and the soil-vegetation system.

and subsequent wetting front calculations, $k(\theta)$ was estimated using the suggestion of Hanks [23] at soil layers bounded by sharp soil moisture content vertical gradients. In such formulation,

$$K_{i-1/2}^{j+1/2} = D_{i-1/2}^{j+1/2} \frac{(\theta_{i-1}^{j} - \theta_{i}^{j})}{(\Psi_{i-1}^{j} - \Psi_{i}^{j})}, \tag{22}$$

where D, the diffusivity, is defined as

$$D_{i-1/2}^{j+1/2} = \frac{\left(\sum_{\theta_L}^{\theta_{i-1}^{j}} (D\Delta\theta) - \sum_{\theta_L}^{\theta_{i}^{j}} (D\Delta\theta) \right)}{(\theta_{i-1}^{j} - \theta_{i}^{j})}, \tag{23}$$

where i and j are depth subscript and time superscript, respectively, and θ_L is the lowest moisture content prior to the precipitation event (see [23] for details). Additionally, we made the following assumptions about the boundary conditions:

(i) The evaporation from the soil surface is negligible relative to the transpiration.

(ii) The water flux at the lower boundary ($z = 0.45$ m) is gravitational.

(iii) The precipitation was reduced using the interception curve (Fig. 4) derived from the measurements reported for grass by Feddes [17] based on the experiment of Rijtema [48]. This interception function, derived by us using the measurements of Rijtema [48], can be expressed by a shifted power law:

$$I_p = 58.56 \times (P_{avg} + 0.3026)^{-0.522}, \tag{24}$$

where I_p is the foliage interception (in %) and P_{avg} is the average precipitation (in mm) for a given storm duration. In (24), the storm duration is defined as the time of sequential non-zero precipitation. Only through-fall enters the flow domain at $z = 0$ before initiating the wetting front calculations. The interception loss estimates were indirectly verified from soil moisture content measurements as discussed in the next section.

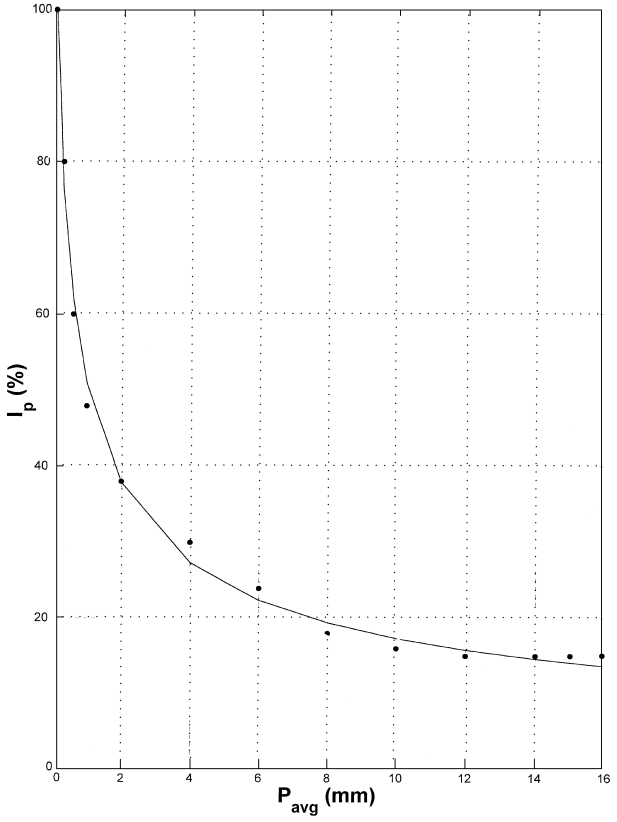

Fig. 4. The precipitation interception (I_p) curve for grass derived from the report of Feddes [17] based on measurements of Rijtema [48]. The dots are the data reported by Feddes and the curve is fitted by a shifted power-law function. The average precipitation (P_{avg}) is computed by averaging the precipitation (P) over the storm duration.

3. Experiments

3.1. Study site

The study site is an *Alta Fescue* grass-covered forest clearing at the Blackwood division of the Duke Forest in Durham, NC. The site is a 480 m × 305 m grass site surrounded by a 10–12 m Loblolly pine stand. The average elevation of the site is 163 m above mean sea level. The measurements were collected from May to July 1997. The grass height (h_c) was 0.7 m at the beginning of the experiment and kept growing up to 1.05 m.

3.2. Meteorological measurements

The required meteorological inputs (mean wind speed V, air temperature T_a, and relative humidity q_a) to compute E_p were measured by a R.M. Young propeller/vane system and a HMP35C temperature/RH Probe, respectively. The surface energy components, net radiation R_n and soil heat flux G, were measured by a Q-7 net radiometer and HFT-3 soil heat flux plate, respectively. All meteorological instruments were installed at height of $z_a = 3.3$ m, while the soil heat flux plate was placed just below the soil surface (0.05 m). The precipitation was measured by a tipping bucket gage (Met One Instruments), situated 15 m from the eddy-correlation tower. The precipitation measurements, reduced to account for interception losses, were used as top boundary conditions for modeling the wetting fronts.

3.3. Turbulence flux measurements

An Applied Technology triaxial sonic anemometer and a Campbell Scientific krypton hygrometer were used to measure latent and sensible heat flux along with the friction velocity. All meteorological and energy components were sampled at 5 Hz with an averaging period of 20 min per run. The surface roughness was determined from near neutral runs using

Table 1
General weather characteristics for the experimental periods

Period	Date (1997)	Cumulative precipitation (mm)	T_a (°C)			RH (%)			V (m s^{-1})			R_n (W m^{-2})
			Max	Min	Avg	Max	Min	Avg	Max	Min	Avg	Max
1	22 May/31 May	9.91	28.9	7.1	18.9	98.3	22.6	72.3	4.32	0.03	1.65	719
2	1 July/10 July	8.89	36.5	15.5	24.8	98.5	26.6	74.8	4.04	0.00	1.15	740

Max: maximum, min: minimum, avg: average.

$$z_o = (z_a - d)\exp\left(\frac{-\kappa V}{u_*}\right), \tag{25}$$

where d is the momentum zero-plane displacement height ($\approx 2/3h_c$) and z_a is the measurement height of the triaxial sonic anemometer. We found that $z_o \approx 0.1h_c$ described well the average behavior though some dependence on wind direction was noted as discussed in Hsieh et al. [25]. Table 1 summarized the general atmospheric and meteorological conditions for the experimental periods.

3.4. Soil properties

The soil texture in the top 0.5 m was decomposed into five layers as shown in Table 2 based on visual observation of soil color while excavating the moisture content trench. During excavation, we also noted that the rock content for this soil was high. A hard clay pan bounding the deeper soil layers (>0.45 m) was also intercepted during the excavation. This clay pan restricted root development beyond 0.45 m depth.

The soil moisture content profile was measured by an array of CS615 water content reflectometers (Campbell Scientific, Logan, UT) close to the meteorological tower. Eight sets of 0.3 m length rods were installed horizontally every 0.05 m depth increment starting from 0.05 to 0.45 m below the ground surface. An additional set was installed vertically to measure the average water content within the root zone. This vertical rod configuration was also used to compute soil moisture storage following a precipitation event to indirectly assess the interception calculations. The 0.3 m rods installed horizontally into the soil-root system ensure strong coupling between the local soil moisture and the integrated root-water uptake from an ensemble of roots crossing that layer.

The averaging time interval for all multiplexed CS615 soil moisture system was 20 min, which synchronized with the meteorological and flux measurements. A compact constant head permeameter (Ksat, Raleigh, NC), which measures the steady-state water flow rate through the soil column, was used to estimate the in situ saturated hydraulic conductivity separately for three soil layers (layers 1, 3, and 5 in Table 2). The saturated soil water content was determined by the highest recorded value following a concentrated precipitation event. The effective values of the empirical parameters b and Ψ_s were selected from Clapp and Hornberger [11] based on soil texture [56] and our measured k_s. Oren et al. [41] reported similar k_s and b values for soils in an adjacent pine forest site. The values for the clay pan ($z > 0.45$ m) in their study, determined from drainage experiments, were very close to the values used in this study. However, in the top 0.3 m, root diameter of pine trees is much larger than grass' resulting in an "apparent" coarser soil texture and a lower b value as expected [29]. Petersson et al. [44] conducted an extensive experiment to study the influence of root mass on saturated hydraulic conductivity in arid soils. They found that a strong positive linear relationship between k_s and root mass was obtained in a well-developed root systems, but not in younger plantations. Such an adjustment to our soil hydraulic properties was not considered.

4. Results and discussion

The experiment duration (22 May–10 July 1997) coincided with maximum grass growth for which increase in grass height can be visually noted. Two drying cycles (22–31 May) and (1–10 July) were selected to evaluate

Table 2
Soil hydraulic properties used in soil-vegetation system

Depth (cm)	Soil texture	K_s (cm d^{-1})	θ_s (cm^3 cm^{-3})	$\lvert\psi_s^a\rvert$ (cm)	b [a]
0–16	Silt loam	15.1	0.30	32.0	4.0
17–22	Loam	5.1	0.38	10.0	4.5
24–33	Silt clay loam	5.5	0.45	62.6	6.5
34–37	Silt clay	3.5	0.56	20.0	7.0
38–45	Clay	1.5	0.63	30.0	10.6

[a]Data reference: Clapp and Hornberger [11].

the proposed theoretical framework because these periods had complete soil moisture content measurements and continuous meteorological and eddy-correlation measurements. Additionally, both periods experienced comparable total precipitation input (9.91 and 8.89 mm, respectively).

In this section, the observed relationship between E_p and E_{act} at the field-case is considered using eddy-correlation measurements, and at the local scale using depth-averaged temporal soil moisture changes along with (4). The measured E_{act}/E_p relationship permits us to assess whether the main root-uptake mechanisms described in (9) are significant at both spatial scales.

To model the observed relationship between E_p and E_{act} using the theoretical framework described in Section 2.2, the parameters (c, γ) of the root-density and efficiency function must be determined. How well the model independently reproduced the observed E_{act}/E_p and $\theta(z,t)$ is also discussed.

4.1. Relationship between E_{act} and E_p

Using the Penman–Brutsaert estimated E_p, the eddy-correlation measured "field-scale" E_{act}, and the estimated "local scale" E_{act} (hereafter referred to as S_m) from (4), the relationship between E_p and E_{act} is

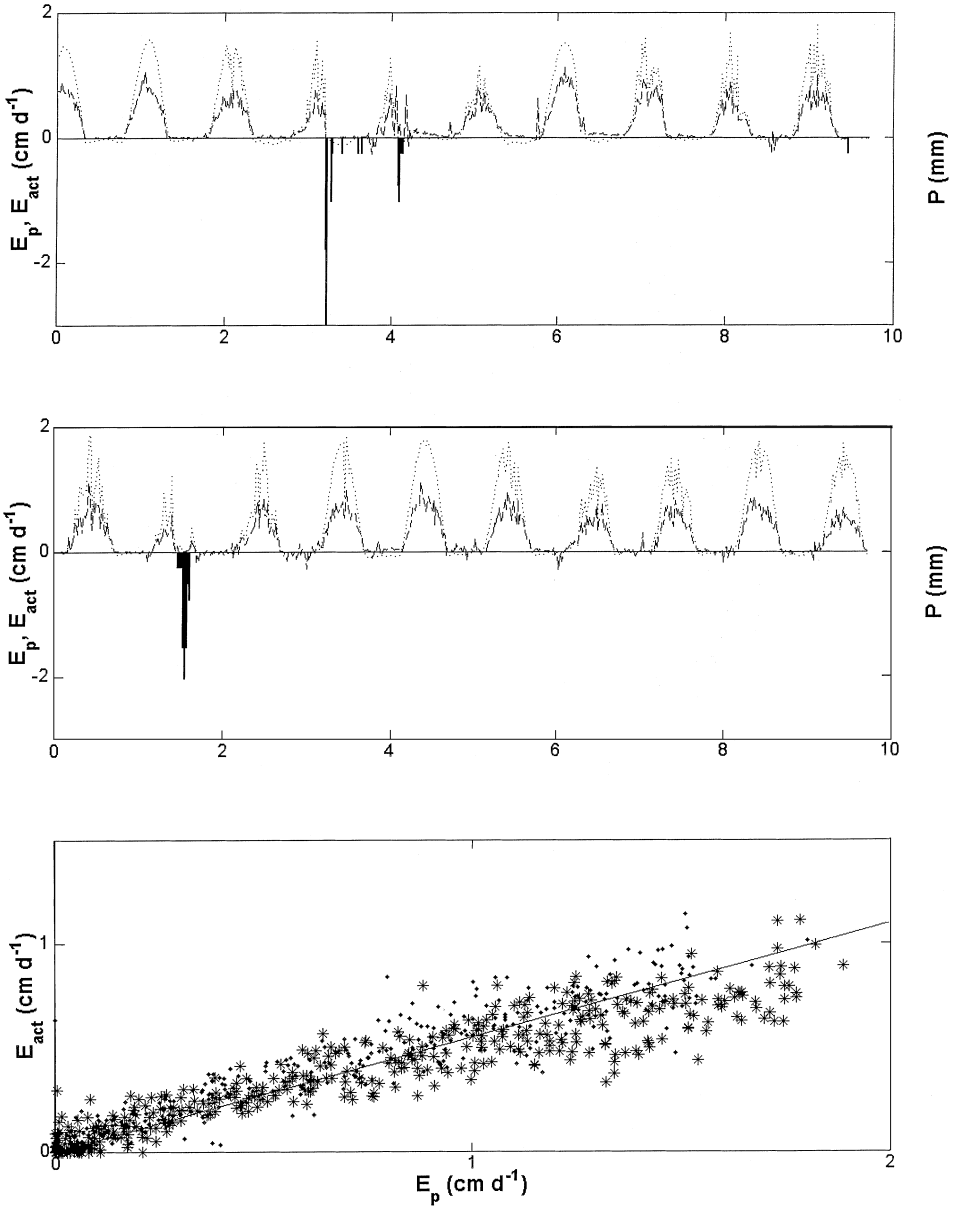

Fig. 5. Diurnal variation of measured E_{act} (dashed) by the eddy-correlation method and calculated E_p (dot) by Penman–Brutsaert model for period 1 (top-panel) and period 2 (middle-panel). The measured precipitation distribution is also shown for reference. The constant E_{act}/E_p (bottom-panel) is demonstrated using the E_{act} measurements from period 1 (dot) and period 2 (star). The solid line is $0.55E_p$.

investigated. In Fig. 5, the variation of measured P, eddy-correlation measured E_{act} and computed E_p is shown for the two periods along with the relationship between E_{act} and E_p. In Fig. 6, a similar relationship is shown between cumulative water uptake derived from (4) and E_p for both periods. Notice that the eddy-correlation measured E_{act} is 60% larger than S_m measured from soil moisture changes (local-scale) for both periods. Given the small changes in soil moisture, such a comparison could not be performed on a 20 min time step.

From Figs. 5 and 6, it is evident that E_{act}/E_p ($=\beta$) is approximately constant but scale dependent for both periods. Using linear regression analysis, β is 0.55 for the eddy-covariance measurements (see Fig. 5), and 0.33 for the soil moisture measurements (see Fig. 6). Hence, whether a large-scale atmospheric perspective or a local-scale soil perspective is adopted, β appears to be nearly constant for the range of soil moisture content variations encountered in this experiment. We investigate possible mechanisms responsible for such a constant β using the proposed formulation. Before we proceed, the two model constants must be determined.

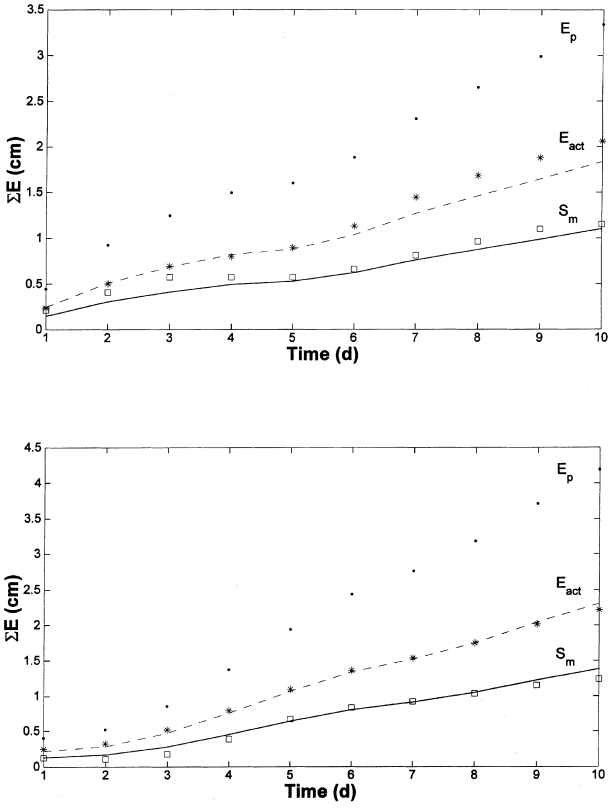

Fig. 6. Comparison between cumulative E_p and E_{act} for period 1 (top) and period 2 (bottom). The E_p (dot), E_{act} (star), and S_m (square) are from model calculations, eddy-correlation measurements, and CS615 measurements, respectively. The $0.55E_p$ and $0.33E_p$ are plotted in dashed and solid lines to illustrate the constant β observed at both spatial scales.

4.2. Model parameter estimation

The empirical root-density and efficiency functions introduce two empirical constants: the slope parameter c (or a) in (10) and the empirical parameter γ in (13) that must be determined prior to estimating root-water uptake. A multi-dimensional optimization was performed using the measurements for period 1 to determine c (or a) and γ. These optimized parameters are independently tested for period 2. The optimization objective function is defined by minimizing the mean squared error (MSE):

$$\mathrm{MSE} = 100 \times \int_{t=t_i}^{t=t_k} \int_{z=0}^{z=L} [S(z,t) - \hat{S}(z,t)]^2 \, \mathrm{d}z \, \mathrm{d}t, \tag{26}$$

where t_i is the time just after an intensive precipitation event and t_k is time at the end of period 1 ($\sim$5 dry-down days for period 1 as evidenced by Fig. 5), $S(z,t)$ is modeled root-water uptake at depth z and $\hat{S}(z,t)$ is the root-uptake calculated from (1) using measured θ and estimated q. In Fig. 7, the variation in MSE with simultaneous variation in c and γ is shown. It is evident from Fig. 7 that the MSE is much more sensitive to variation in γ (root-efficiency) when compared to variations in c (root density). Interestingly, the optimum γ is close to its expected 0.01 value as discussed in Section 2.2.2. At $\gamma = 0.01$, the MSE was robust to c variations for $c \in [0,-0.7]$. Additionally, $g(z)$ of Jackson et al. [27] along with optimization on the parameter a was considered. The optimization results indicate that the minimum MSE for the $g(z)$ model of Jackson et al. [27] is 2.5 times larger than the Hoogland et al. model [24] if a 0.35 m root-zone depth is used. The apparent failure of Jackson et al. model [27] is attributed to the

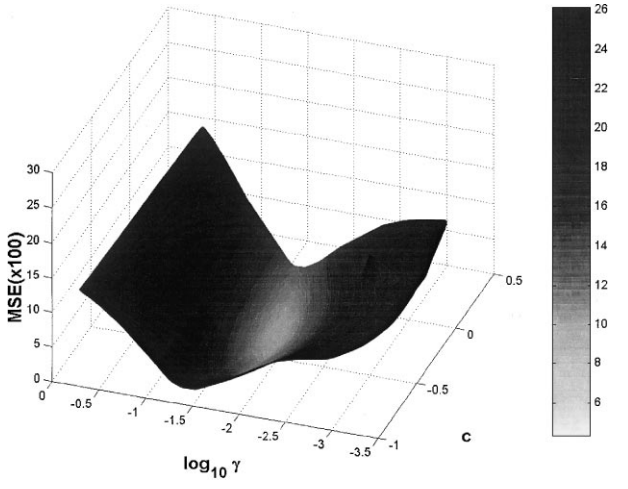

Fig. 7. Variation in MSE for period 1 as a function of model parameters c and γ. The optimization resulted $\gamma = 0.01$ and was insensitive to c for a wide range of c values.

large reduction in $g(z)$ for $z > 0.2$ m; hence, only a small percentage of the efficient deep-roots are permitted to contribute to E_{act}. A comparable MSE can be obtained if in (10(b)), the root-zone depth is extended to 0.9 m thus increasing the percentage of deep roots. Because of the hard clay pan below 0.45 m, such a deep rooting zone is rather unrealistic. We do not claim that the linear root-density model of Hoogland et al. [24] is more realistic than the power-law function of Jackson et al. [27] as an absolute descriptor of root density but rather that the root efficiency $\alpha(\theta)$ is much more important than $g(z)$ for field conditions encountered in this experiment. Hence, for the remaining discussion, the near-optimum empirical constants are $c = -0.5$ and $\gamma = 0.01$.

4.3. Soil moisture content comparisons

Using $c = -0.5$ and $\gamma = 0.01$, a comparison between measured and modeled θ is shown in Fig. 8 for both periods. It is important to note that while the cumulative precipitation are nearly identical for both periods, the temporal distribution is not. For the second period, P is rather concentrated in time (~3.5 h) when compared to

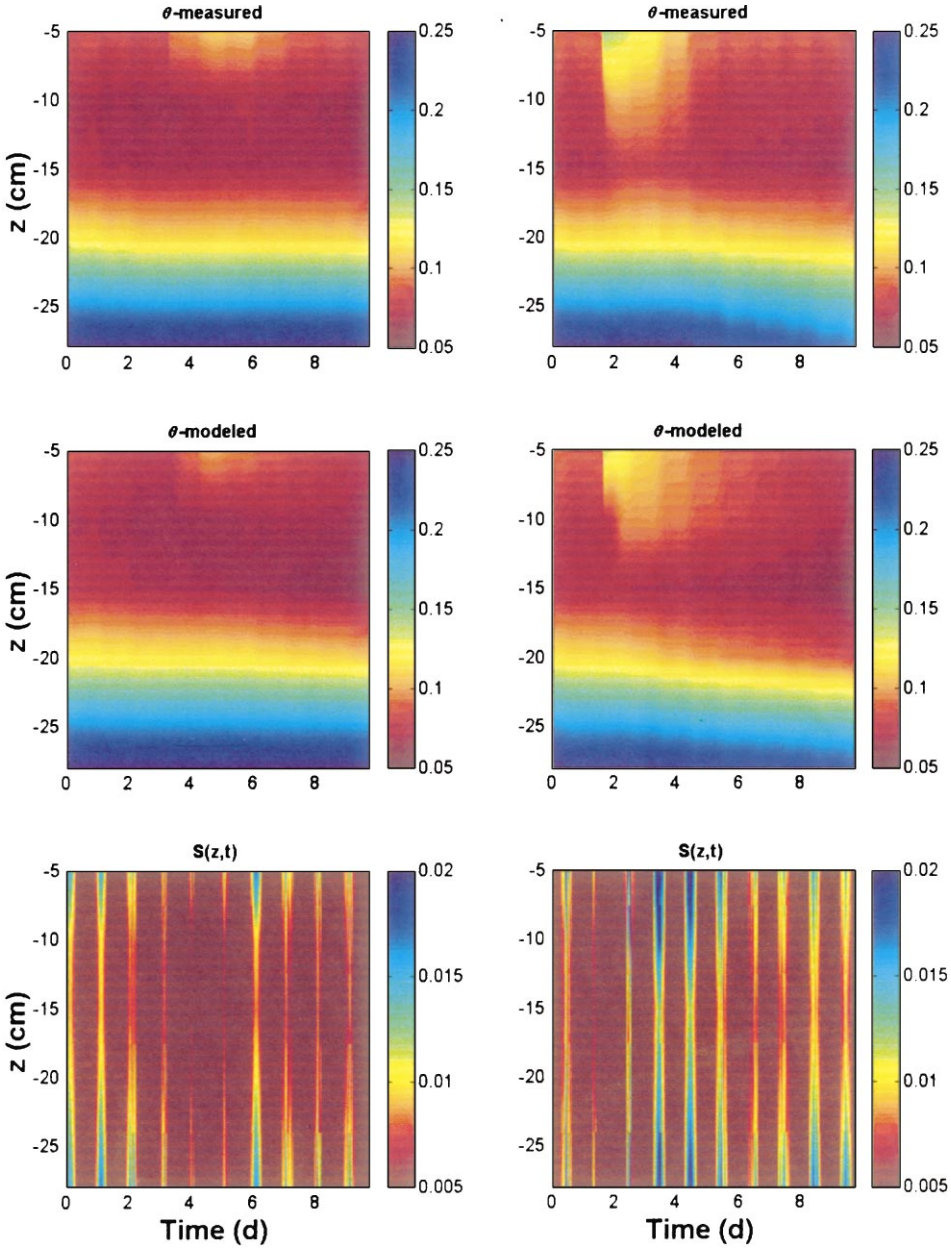

Fig. 8. Comparison between measured (top-panels) and modeled (middle-panels) soil moisture content profiles for period 1 (left-column) and period 2 (right-column) using the optimized c and γ values from period 1. The modeled $S(z,t)$ is also shown (bottom-panel) for both periods.

the first period (~1.0 d) as evidenced by Fig. 5. As such, the interception losses in the first period (~85%) are much larger than the second period (~55%). The differences in interception losses between the two periods are realized in patterns of measured near-surface $\theta(z,t)$ (Fig. 8 top figures). During a precipitation event, $S(z,t) \approx 0$ and the ability of the model to reproduce measured θ is primarily dependent on the soil hydraulic properties. Hence, the good agreement between measured and modeled θ as the wetting front progresses (see Fig. 8) suggests that the choice of hydraulic properties (see Table 2) is reasonable and adequate to model the drying patterns discussed next.

When $S(z,t) > 0$, the model captures the basic drying patterns at different soil layers; however, in certain near-surface regions, discrepancies are apparent, particularly in water uptake following the precipitation event for period 2 (see Fig. 8). The observed rapid drying pattern in the 0.05–0.15 m layers is larger than model prediction. There are several potential explanations for such underestimation; however, it must be emphasized that for such a stratified soil, the vertical variability in θ is much larger than the temporal variability for any given layer. Also, the coloring scheme in Fig. 8 is chosen to amplify differences in measured and modeled θ near the surface. In fact, these differences are of the order of 0.03 cm^3 cm^{-3} and are well within the CS615 calibration error [29,41]. The fact that the model was able to reproduce much of the observed $\theta(z,t)$ for both periods (especially for the deeper soil layers) permits us to investigate the primary mechanisms responsible for the observed near constant β using model calculated S.

The calculated $S(z,t)$ is also shown in Fig. 8 for both periods (bottom-panel). Based on the modeled $S(z,t)$, the following can be noted (specifically for period 2):

(1) Directly following the precipitation event, the top layers (0–0.2 m) rapidly uptake water in direct proportion to the root density. The deeper layers (0.2–0.35 m) continue to uptake water but not at the same strength as the top layer.

(2) As moisture content approaches near-wilting point in the top layers, the deeper layers become the main contributors to E_{act}.

Based on these two results, we deduce the following:

(1) The rooting-system preferentially uptake water from the top layers if the water is freely available.

(2) The deeper layers are able to extract water at a high rate. These findings are in excellent qualitative agreements with heat pulse measurements within Kiwifruit vines rooting reported by Green and Clothier [22] and dry weight root measurements for turf grasses reported by Huang et al. [26]. Both studies conclude that roots are able to preferentially uptake water from the near surface when water is freely available, but are able to adjust to near-surface drought by uptaking water from deeper layers. The transition from shallow-layer to deeper layer uptake occurs within days. They also found that root viability (which is a physiological function) is more critical than the root length density. Sala et al. [50] also demonstrated a shifted root water extraction from shallow to deep soil layers in a shortgrass study for a long drying cycle. They proposed that the gradual shift be related to the distribution of water potentials within the soil and the pattern of daily dynamics in leaf water potential. They also concluded that in the dryer (surface) layer, the water flow to the rooting system is restricted because of a small soil-leaf water potential gradient; in the wetter (deeper) layers, the flow is somewhat more limited by the lack of sufficient root length density. Our model indirectly accounts for such observations by forcing the deeper layers to uptake water more efficiently when compared to the surface soil as in (12) but allocate more rooting density to the top layers via $g(z)$. In summary, the proposed root efficiency functions in (12) and (13) permit such uptake adjustment from shallow to deeper layers when near-surface $\theta \to \theta_w$; meanwhile, it allows the near-surface roots to preferentially uptake water for large θ. Hence, the model mirrors the relative contribution of these two layers to

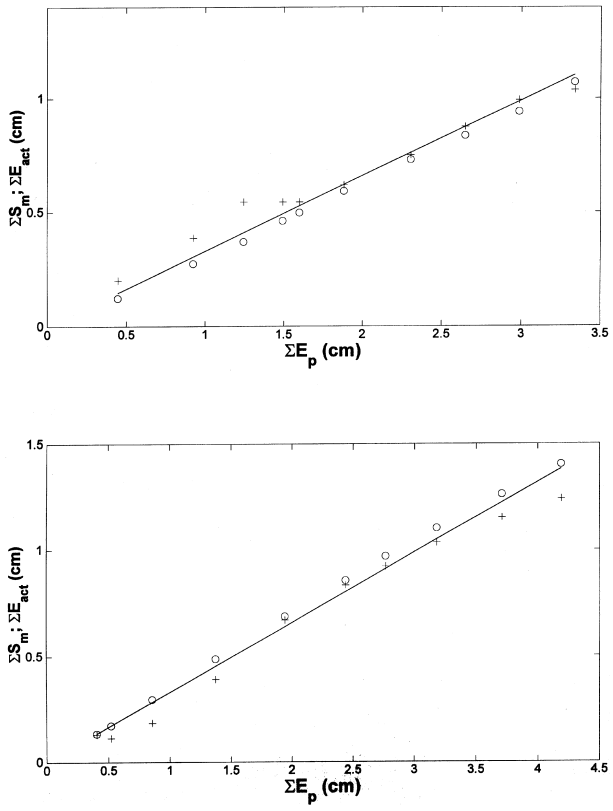

Fig. 9. Variation in cumulative E_{act} as a function of cumulative E_p for period 1 (top) and period 2 (bottom). Open circles represent calculated E_{act} from modeled $S(z,t)$, and plus symbols represent estimated S_m using CS615 measurements for θ. The solid line is $0.33E_p$.

E_{act} as the drying cycle progresses. We consider next whether the modeled E_{act} preserves the near constant β shown in Fig. 9(a) and (b).

4.4. Model validation of E_{act}/E_p

Using (2), (8) and computed E_p, Fig. 9(a) and Fig. 9(b) display the variations of cumulative E_{act} as a function of cumulative E_p for both periods. The solid lines represent $E_{act} = 0.33E_p$. While the good agreement between measured and modeled E_{act}/E_p is not surprising for period 1 given that the parameters are optimized to match observed $S(z,t)$, the good agreement for period 2 cannot be attributed to such optimization artifacts. We iterate again that the model calculations were not forced to produce a constant E_{act}/E_p; however, the modeled near constant β of Fig. 9(b) was the result of deeper root contribution to E_{act}.

5. Conclusion

This study investigated the role of root-water uptake on the E_{act}/E_p relationship experimentally and numerically. A model linking atmospheric demand (via potential evaporation) to soil moisture redistribution in the presence of a root system was developed. The Penman–Brutsaert potential evaporation model, a moisture-dependent root efficiency function and a linear root-density function were used to model water movement within the soil-vegetation-atmosphere continuum. Based on the measurements and model calculations, we concluded the following:

(1) The measured E_{act}/E_p at the field scale ($=0.55$ using eddy-correlation measurements) and the local scale ($=0.33$ using soil moisture content measurements) suggest a near constant β for both drying periods. Hence, the root-dynamics responsible for such a constant β are not dependent on the measurement spatial scale and their influence is sensed at both local and field scales.

(2) The proposed root efficiency function along with a linear root-density distribution provides a parsimonious model to describe root-water uptake. When coupled with Richards' equation, the proposed root-water uptake model reproduces well measured time-depth soil moisture content dynamics within the root zone.

(3) The root-uptake model captures well preferential water uptake from the top layers when water is freely available and is able to permit high extraction rates from deeper layers despite limited rooting density in those layers. While the model does not explicitly treat water uptake transition from shallow to deeper layers as observed by Green and Clothier [22] and Huang et al. [26], it does provide a practical solution to account for the dynamic switching of root water extraction as a function of soil moisture content. Hence, the model indirectly mirrors the relative contribution of root-water uptake at different depths to the over all E_{act}. In fact, the computed β by such model is nearly constant and is in close agreement with the local β measurements for both periods.

The broader implication of this study, when considered in concert with Green and Clothier [22] and Huang et al. [26], is that vertical root-density distribution cannot be the primary variable used to allocate water uptake at different soil layers. Such root-water allocation has been used in many recent GCM model runs (e.g. [14]). In fact, the root viability reflected by root-water uptake efficiency can be equally critical (if not more important) for many vegetation types.

Acknowledgements

The authors would like to thank Fred Mowry and David Ellsworth for lending us some of the micrometeorological instruments. The authors would also like to thank Shang-Shiou Li for his help in setting up the experiment. This study was supported, in part, by the Department of Energy FACTS-I project (DOE Cooperative Agreement No. DE-FG05-95 ER 62083) and National Science Foundation (NSF-BIR-9512333).

References

[1] Alaerts M, Badji M, Feyen J. Comparing the performance of root-water-uptake models. Soil Sci 1985;139(4):289–96.
[2] Andre J-C, Goutorbe J-P, Perrier A. HAPEX-MOBILHY: A hydrologic atmospheric experiment for the study of water budget and evaporation flux at the climatic scale. Am Meteorol Soc 1986;67(2):138–44.
[3] Belford RK, Klepper B, Rickman RW. Studies of intact shoot-root systems of field-grown winter wheat. II. Root and shoot developmental patterns as related to nitrogen fertilizer. Agron J 1989;79:310–19.
[4] Blum A, Ritchie JT. Effect of soil surface water content on sorghum root distribution in the soil. Field Crops Res 1984;8:169–76.
[5] Brutsaert W. Evaporation into the atmosphere: Theory, history, and applications. Dordrecht, The Netherlands: Kluwer Academic Publishers, 1982:209–30.
[6] Brutsaert W, Parlange MB. The unstable surface-layer above a forest: Regional evaporation and heat flux. Water Resour Res 1992;28:3129–34.
[7] Budyko MI. The heat balance of the earth's surface. English translation by US Department of Commerce, Weather Bureau, 1956.
[8] Businger J. A note on the Businger–Dyer profiles. Bound Layer Meteorol 1988;42:145–51.
[9] Cahill AT, Parlange MB. On the Brutsaert temperature roughness length model for sensible heat flux estimation. Water Resour Res 1997;33:2315–24.
[10] Campbell GS. A simple method for determining unsaturated conductivity from moisture retention data. Soil Sci 1974;117:311–4.

[11] Clapp RB, Hornberger GM. Empirical equations for some soil hydraulic properties. Water Resour Res 1978;14:601–4.
[12] Clausnitzer V, Hopmans JW. Simultaneous modeling of transient three-dimensional root growth and soil water flow. Plant Soil 1994;164:299–314.
[13] Clothier BE, Green SR. Roots: The big movers or water and chemical in soil. Soil Sci 1997;162:534–43.
[14] Dickinson RE, Henderson-Sellers A, Kennedy PJ. Biosphere-atmosphere transfer scheme (BATS) version le as coupled to the NCAR community climate model. NCAR technical note 1993, NCAR/TN-387+STR.
[15] Dyer AJ. A review of flux-profile relationships. Bound Layer Meteorol 1974;7:363–72.
[16] Ellis FB, Barnes BT. Growth and development of root systems of winter cereals grown after different tillage methods including direct drilling. Plant Soil 1980;55:283–95.
[17] Feddes RA. Water, heat and crop growth. Mededelingen, Wageningen, The Netherlands, 1971:57–72.
[18] Feddes RA, Kowalik P, Kolinska-Malinka K, Zaradny H. Simulation of field water uptake by plants using a soil water dependent root extraction function. J Hydrol 1976;31:13–26.
[19] Feddes RA, Kowalik PJ, Zaradny H. Simulation of field water use and crop yield. Simulation Monograph, Pudoc, Wageningen, The Netherlands, 1978:9–30.
[20] Feddes RA, Kabat P, Van Bakel PJT, Bronswijk JJB, Halbertsma J. Modelling soil water dynamics in the unsaturated zone – state of the art. J Hydrol 1988;100:69–111.
[21] Glinski J, Lipiec J. Soil physical conditions and plant roots. Boca Raton, FL:CRC Press, 1990.
[22] Green SR, Clothier BE. Root water uptake by kiwifruit vines following partial wetting of the root zone. Plant Soil 1995;173:317–28.
[23] Hanks RJ. Infiltration and redistribution. Modeling plant and soil systems. Madison, WI (USA), ASA-CSSA-SSSA, 1991:181–203.
[24] Hoogland JC, Feddes RA, Belmans C. Root water uptake model depending on soil water pressure head and maximum extraction rate. Acta Hort 1981;119:123–36.
[25] Hsieh CI, Katul GG, Schieldge J, Sigmon JT, Knoerr KK. The lagrangian stochastic model for fetch and latent heat flux estimation above uniform and nonuniform terrain. Water Resour Res 1997;33:427–38.
[26] Huang B, Duncan RR, Carrow RN. Drought-resistance mechanisms of seven warm-season turfgrasses under surface soil drying: II. Root Aspects. Crop Sci 1997;37:1863–69.
[27] Jackson RB, Canadell J, Ehleringer JR, Mooney HA, Sala OE, Schulze ED. A global analysis of root distributions for terrestrial biomes. Oecologia 1996;108:389–411.
[28] Katul GG, Parlange MB. A Penman–Brutsaert model for wet surface evaporation. Water Resour Res 1992;28:121–26.
[29] Katul GG, Todd P, Pataki D, Kabala ZJ, Oren R. Soil water depletion by oak trees and the influence of root water uptake on the moisture content spatial statistics. Water Resour Res 1997;33:611–23.
[30] Kleidon A, Heimann M. Optimized rooting depth and its impacts on the simulated climate of an atmospheric general circulation model. Geophys Res Lett 1998;25(3):345–48.
[31] Kutilek M, Nielsen DR. Soil hydrology. Germany: Catena Verlag, 1994:195–216.
[32] Lynn BH, Carlson TN. A stomatal resistance model illustrating plant vs. external control of transpiration. Agric For Meteorol 1990;52:5–43.
[33] Mason WK, Rowse HR, Bennie ATP, Kaspar TC, Taylor HM. Responses of soybeans to two row spacings and two soil water levels. II. Water use, root growth, and plant water status. Field Crop Res 1982;5:15–29.
[34] Milly PCD. Sensitivity of greenhouse summer dryness to changes in plant rooting characteristics. Geophys Res Lett 1997;24(3):269–71.
[35] Molz FJ, Remson I. Extraction term models of soil moisture use by transpiring plants. Water Resour Res 1970;6:1346–56.
[36] Molz FJ. Models of water transport in the soil-plant system: A review. Water Resour Res 1981;17:1245–60.
[37] Nepstad DC, Decarvalho CR, Davidson EA et al. The role of deep roots in the hydrological and carbon cycles of Amazonian forests and pastures. Nature 1994;372:666–9.
[38] Nimah MN, Hanks RJ. Model for estimating soil water, plant and atmospheric interrelations. I. Description and sensitivity. Soil Sci Soc Am Proc 1973a;37:522–7.
[39] Nimah MN, Hanks RJ. Model for estimating soil water, plant and atmospheric interrelations. II. Field test of model. Soil Sci Soc Am Proc 1973b;37:528–32.
[40] Novak V. Estimation of soil water extraction patterns by roots. Agric Water Mgt 1987;12:271–8.
[41] Oren R, Ewers BE, Todd P, Phillips N, Katul G. Water balance delineates the soil layer in which moisture affects canopy conductance. Ecological Appl 1998;8:990–1002.
[42] Penman HL. Natural evaporation from open water, bare soil and grass. Proc R Soc London, Ser A, 1948;193:120–46.
[43] Perrochet P. Water uptake by plant roots – a simulation model, I. Conceptual Model. J Hydrol 1987;95:55-61.
[44] Petersson H, Messing I, Steen E. Influence of root mass on saturated hydraulic conductivity in arid soils of central Tunisia. Arid Soil Res Rehabil 1987;1:149–60.
[45] Prasad R. A linear root water uptake model. J Hydrol 1988;99:297–306.
[46] Protopapas AL, Bras RL. Effects of weather variability and soil parameter uncertainty on the soil-crop-climate system. Am Meteorol Soc 1992;6:645–56.
[47] Radcliffe D, Hayden T, Watson K, Crowley P, Phillips RE. Simulation of soil water within the root zone of a corn crop. Agron J 1980;72:19–24.
[48] Rijtema PE. An analysis of actual evapotranspiration. Agric Res Rep, Pudoc, Wageningen, 1965;659:107.
[49] Ritchie JT. A user-oriented model of the soil water balance in wheat. USDA-ARS, Grassland, Temple, Tex.: Soil and Water Res Lab, 1984:21.
[50] Sala OE, Lauenroth WK, Parton WJ, Trlica MJ. Water status of soil and vegetation in a shortgrass steppe. Oecologia 1981;48:327–31.
[51] Schmidhalter U, Selim HM, Oertli JJ. Measuring and modeling root water-uptake based on chloride-36 discrimination in a silt loam soil affected by groundwater. Soil Sci 1994;158(2):97–105.
[52] Shein EV, Pachepsky YA. Influence of root density on the critical soil water potential. Plant Soil 1995;171:351–7.
[53] Somma F, Hopmans JW, Clausnitzer V. Transient three-dimensional modeling of soil water and solute transport with simultaneous root growth, root water and nutrient uptake, Plant Soil, 1998;202:281–93.
[54] Taylor HM, Klepper B. Rooting density and water extraction patterns for corn (Zea mays L.), Agron J 1973;65:965–8.
[55] Taylor HM, Klepper B. Water uptake by cotton root systems: an examination of assumptions in the single root model. Soil Sci 1975;120:57–67.
[56] Van Bavel CHM, Stirk GB, Brust KJ. Hydraulic properties of a clay loam soil and the field measurement of water uptake by roots:

I. Interpretation of water content and pressure profiles. Soil Sci Soc Am Proc 1968;32:310–7.

[57] Wetzel PJ, Chang JT. Concerning the relationship between evapotranspiration and soil moisture. J Clim Appl Meteorol 1987;26:18–27.

[58] Zeng X, Dai YJ, Dickinson RE, Shaikh M. The role of root distribution for climate simulation over land. Geophys Res Lett 1998;25(24):4533–6.